11th Australasian Fluid Mechanics Conference
University of Tasmania, Hobart, Australia
14-18 December 1992

SHEAR AND INSTABILITY IN THE FLOW DRIVEN BY A SHOALING INTERNAL WAVE

J.R. TAYLOR

Centre for Water Research
University of Western Australia
Nedlands, WA 6009, AUSTRALIA

Abstract

The conditions under which turbulent mixing occurs as an internal wave breaks on a slope have been studied in a laboratory experiment. Mode one (in the vertical) internal waves were generated by a centrally located wave paddle and propagated toward parallel sloping endwalls. Measurements were made of the vertical density profile and horizontal velocity through the mixing layer that formed along the slope as the waves broke. It was found that the minimum vertically averaged gradient Richardson number occurred when the stratification was minimum and the shear maximum. The association of high shear and low density gradient contrasts with the more common situation in a stratified flow where shear instability occurs when there is a high shear across a density interface.

Introduction

In a number of stratified lakes Imberger (1989) found that mean vertical diffusion rates could not be reconciled with observations of vertical turbulent mixing in the interior. As a result, he suggested that most mixing occurs at the boundary and that changes in the interior density profile result from the vertical advection of the mean density structure to balance the lateral buoyancy gradients induced by boundary mixing processes. This mixing may be driven either by shear driven turbulence in the boundary layer or by turbulence resulting from overturning motions which may occur as internal waves shoal along the sloping boundaries of the water body.

Internal waves breaking on a slope have been modelled in previous laboratory experiments in a continuous stratification by Ivey and Nokes (1989) and Taylor (1992). In the second of these it was shown that the overturning length scales and buoyancy anomalies in density inversions within the mixing layer at the boundary varied strongly during the period of the incident wave. To define the overturn length scale measured density profiles were resorted so that they increased monotonically with depth (Thorpe, 1977). The displacements of the density samples moved in the reordering, l_i, were recorded and the displacement scale, l_d, calculated as the r.m.s. value of l_i through the depth of the mixing layer. The buoyancy anomaly, g', was taken to be the r.m.s. buoyancy difference between the resorted and original profiles (Imberger and Ivey, 1991) over the same depth interval.

The measurements of g' and l_d reported in Taylor (1992) suggest that the turbulence grows and decays during each wave period, however, they give little understanding of the conditions under which the transition to turbulence (hence mixing) occurs. In the present work the evolution of the velocity shear in the boundary layer during the wave cycle is examined. Along with vertical profiles of density gradient, shear measurements allow the dynamic stability of the flow to be described in terms of the gradient Richardson number (Turner, 1979),

$$Ri = N^2 / \left(\frac{\partial u}{\partial z}\right)^2 \qquad (1)$$

where $N^2 = -(g/\rho_0)(\partial\rho/\partial z)$ is the local value of the buoyancy frequency squared ($\partial\rho/\partial z$ is the vertical component of the density gradient) and $\partial u/\partial z$ is the vertical gradient of the horizontal velocity in the along-tank direction. The measurements made during the experiments suggest that initially the mixing is not driven purely by shear in the boundary layer but that the overturning of the isopycnals by the wave-induced mean flow is important as well. Thus, the internal wave breaking in these laboratory experiments is consistent with the observation of convective-like temperature structure in the oceanic bottom boundary layer on a continental slope by Thorpe *et al.* (1991). However, by contrasting the results of experiments at different forcing amplitudes, it appears that shear in the attached upslope boundary layer flow is important in maintaining turbulence and mixing after the initial period of mixing-layer scale overturning.

Experiments

The experiments were performed in a tank 5900 mm long by 535 mm wide filled with an approximately linear salinity stratification using the two-tank method. The typical value of N^2 was $0.22\,\mathrm{s}^{-2}$ and depth was 532 mm. At either end of the tank fixed acrylic beaches, set at an angle of 20° to the horizontal, were placed so that the enclosed volume of the tank formed a parallelogram as in Ivey and Nokes (1989). Vertical mode 1 internal waves were generated by a centrally hinged paddle which was located in the middle of the tank and driven by a computer controlled stepper motor.

Vertical profiles of conductivity and temperature were acquired using a PME 4-electrode micro conductivity cell (Head, 1983) and a Thermometrics FP07 fast response

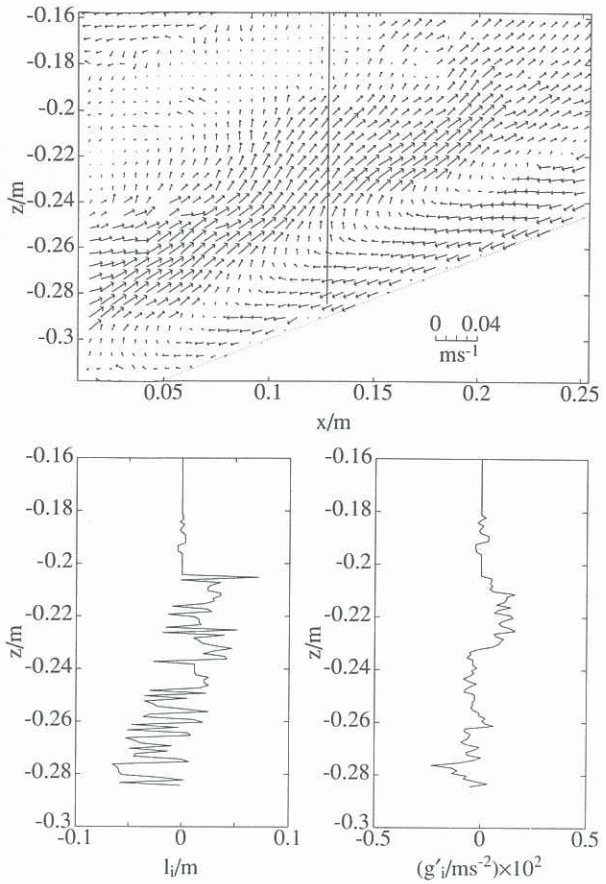

Fig. 1. Velocity field derived from a pair of particle images captured during a run with 10° paddle amplitude. The solid vertical line in the vector plot shows the position of the vertical profiles. The two lower panels show the sample displacements, l_i, and buoyancy anomalies, g_i', computed from the corresponding density profile.

thermistor. The profiles were recorded $0.46L$ (where L is the length of the slope) from the point where the slope intersected the bottom of the tank. Profiles were taken at a time interval of 80 s compared to the forced wave period, T, of 39 s (for all runs) so that there was a phase difference (relative to the forced wave) of 0.32 rad (18.5°) between the profiles. A series of 22 profiles were acquired in each run so that the full phase of the flow on the slope was sampled. The sensors were traversed vertically at 0.1 ms^{-1} with direct and differentiated outputs from the thermistor and conductivity probes being logged at 100 Hz.

Simultaneous with the profiling, wave breaking was visualised by recording, with a CCD video camera, the images of "pliolite" particles suspended in the water column. The particles were illuminated by an approximately 10 mm thick vertical light sheet generated by a 4.0 W argon-ion laser. The microcomputer which controlled the acquisition of the profile data was set up so that it would trigger the acquisition of three frames of video, each separated by two video frame periods (0.08 s) immediately before the probes came into the field-of-view of the camera. Pairs of these frames were later analysed to compute the two-dimensional velocity field using the cross-correlation between windows of 20 by 20 pixels (7 × 7 mm) (Stevens and Coates, 1991; Willert and Gharib, 1991) centred on a grid with spacing eight pixels (3 mm). The area imaged was 254 × 177 mm.

Runs were made at paddle amplitudes (defined by half of the paddle's total angular displacement) of 7°, 10° and 13°. Three runs were made at each amplitude. With the incident wave period of 39 s, the nominal angle of the wave group velocity, defined by $\sin^{-1}(2\pi/TN)$ (Turner, 1979), was 20.1° to the horizontal, compared to the beach angle of 20°. In the final run the stratification had weakened so that the wave angle was 21.3°. As a result, the forcing frequency was a maximum of 7% from the critical condition where the wave group velocity vector and bottom slope are parallel.

Results

An overall description of the flow generated by a wave breaking on the beach has been given in Taylor (1992). Briefly, during each wave period the flow evolves in the following way. A previous wave leaves a strongly sheared, although apparently laminar, downslope flow along the boundary. The next incident wave is first seen as an upslope flow which rides over the downslope boundary layer. The interaction of the up and downslope flows sets up an unstable density profile with associated displacements comparable with the thickness of the two regions (Fig. 1). After the downslope flow is arrested the upslope flow becomes attached to the boundary. It then decelerates and eventually stagnates as the maximum up slope excursion is reached, leaving a field of weakly overturning eddies. The downslope boundary layer then reforms as the elevated heavy fluid accelerates back towards its level of neutral buoyancy.

For each vertical density profile a snapshot of the x (along tank) and z (vertical) components of velocity (in the same plane as the density profiles) was calculated from a pair of particle images. Since it took 1.8 s for the profiler to traverse the field of view of the camera, at worst (at the bottom of the profile) the velocity data was acquired at least that length of time prior to the density data. Given this delay, it seemed more sensible to compute the Richardson number based on the average density and horizontal shear through the depth of the mixing layer, rather than vertical profiles of this parameter. The section of the profiles and velocity fields averaged was defined on the basis of a threshold on the conductivity gradient signal. The choice of the threshold value is discussed in Taylor (1992).

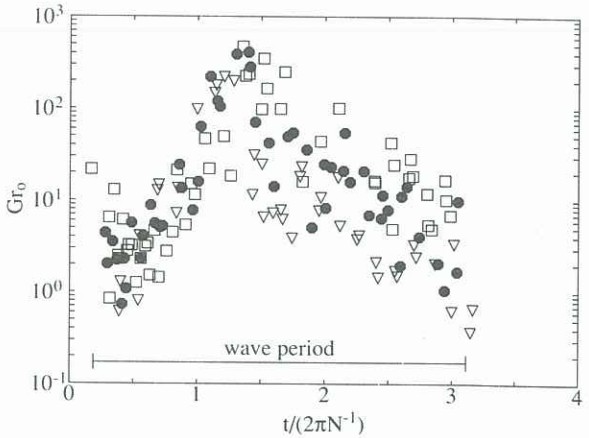

Fig. 2. The average Gr_o for each profile as a function of the phase (in fractions of a buoyancy period) relative to the forced wave. The results for each run have been offset to a common phase origin. Symbols: ▽ paddle amplitude, 7°; • 10°; □ 13°. The horizontal bar shows the dimensionless time for one period of the forced wave at an average value of N.

As background to the Richardson number results the variation in mixing layer averaged overturn Grashof number, Gr_o, during a wave cycle is shown on Fig. 2. This parameter (Taylor, 1992) is defined by

$$Gr_o = \left(\frac{g' {l_d}^3}{\nu^2}\right)^{1/2} \tag{2}$$

where ν is the kinematic viscosity. The overturn Grashof number relates the timescale for restratification of overturned fluid, $(g'/l_d)^{-1/2}$, to the timescale for viscosity to diffuse momentum over the displacement scale, l_d^2/ν. Thus if Gr_o is small viscosity inhibits buoyancy driven restratification. If it is large then restratification may be rapid and it is possible that some of the available potential energy in the density overturns will be utilised in mixing.

Over a wave cycle, and at each amplitude of the incident wave, Gr_o increases to a peak value greater than 100 then decays. For times less than that of the maximum in Gr_o the points for each forcing amplitude tend to overlay, while after the maximum, values are generally ordered as the forcing amplitude. Note that the velocity field and profile shown in Fig. 1 were taken at a dimensionless time of 1.16, just prior to the maximum Gr_o.

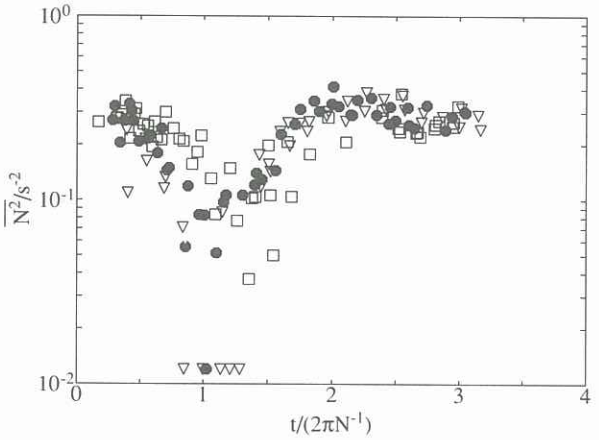

Fig. 3. The average squared buoyancy frequency for each profile. The time axis and symbols are as for Fig. 2. Negative values of $\overline{N^2}$ have been set equal to $0.012\,\mathrm{s}^{-2}$.

Since it is based on g', which is the buoyancy in overturn events, Gr_o scales only the destabilising effects of buoyancy. On the other hand, for positive Richardson number (Eq. 1), buoyancy is stabilising since it counters the torque applied to a (perturbed) fluid element by a vertical gradient of horizontal velocity. Fig. 3 shows $\overline{N^2}$ plotted against the phase of the forced wave. Vertical profiles of N^2 were calculated from density profiles using central differences. The resulting vertical gradients were low-pass filtered with a cut-off at the Nyquist frequency of the velocity data, determined by the grid spacing used in the correlation computations. As for Gr_o the N^2 values presented are averages through the depth of the mixing layer. During the wave cycle the mean stabilising gradient in the mixing layer varies by about a decade. Minimum stability occurs around the time of the maximum in Gr_o (Fig. 2) at 7° and 13° paddle amplitudes, slightly before for the runs at a paddle amplitude of 10°. In the runs at the lowest paddle amplitude the mean gradient was unstable in a

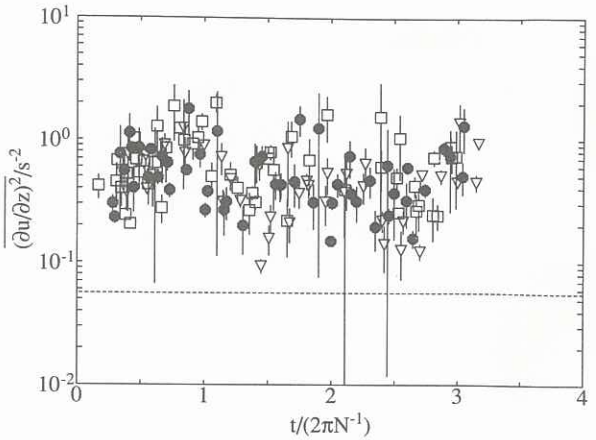

Fig. 4. $\overline{(\partial u/\partial z)^2}$ for each profile. The time axis and symbols are as for Fig. 2. The horizontal dotted line is an estimate of the minimum resolvable shear computed from images of quiescent conditions.

number of cases (for these points $\overline{N^2}$ was set to $0.012\,\mathrm{s}^{-2}$ on Fig. 3).

The mean squared shear (Fig. 4) was calculated from velocity profiles at the four vertical grid lines closest to the position of the density profiles. The calculated velocity profiles were first differenced to compute shear then interpolated on to the same depth axis as the density profiles using splines. These interpolated profiles were low pass filtered using the same filter as used on the density profiles. Given the wavenumber response of the low-pass filter no amplitude correction for the first differencing operation was required. For each profile $\overline{(\partial u/\partial z)^2}$ was computed by averaging $(\partial u/\partial z)^2$ over the same depth range as used in the calculation of $\overline{N^2}$ and Gr_o. The data on Fig. 4 are the average of $(\partial u/\partial z)^2$ from the four grid lines and the error bars are the standard deviation about this mean. Only points from profiles with more than 85% valid velocity points in the depth interval over which the average was calculated were used in the plots.

The variation in mean shear during the wave cycle is far less obvious than is that in the density gradient. Initially (in the downslope phase of the flow) the shear increases and there is no clear trend with incident wave amplitude. There is a decrease in the shear amplitude just later than the time of the minimum density gradient and maximum Gr_o. After the shear minimum the values are somewhat scattered, although they tend to be ordered with forcing amplitude. There is a further weak minimum in shear around $t/(2\pi N^{-1}) = 2.5$, the time when the upslope excursion of fluid is greatest. Following this, shear values tend to coalesce and trend upward as the downslope boundary layer flow is established leading into the next wave cycle.

Although there is some scatter in the points due to variability in the mean shear, a systematic variation in Ri during a wave period is present at each forcing amplitude (Fig. 5). For instance, at all amplitudes, Ri is small or negative as the density gradient approaches its minimum value and the shear its maximum. Soon after the decrease in $\overline{(\partial u/\partial z)^2}$ and increase in $\overline{N^2}$ combine so that Ri increases. In the period when Gr_o is high, when mixing would be expected, Ri tended to be ordered inversely with the forcing amplitude, with the runs at 13° paddle displacement having the lowest Ri (Fig. 5c). Finally, at all amplitudes Ri is maximum around the time when the upslope

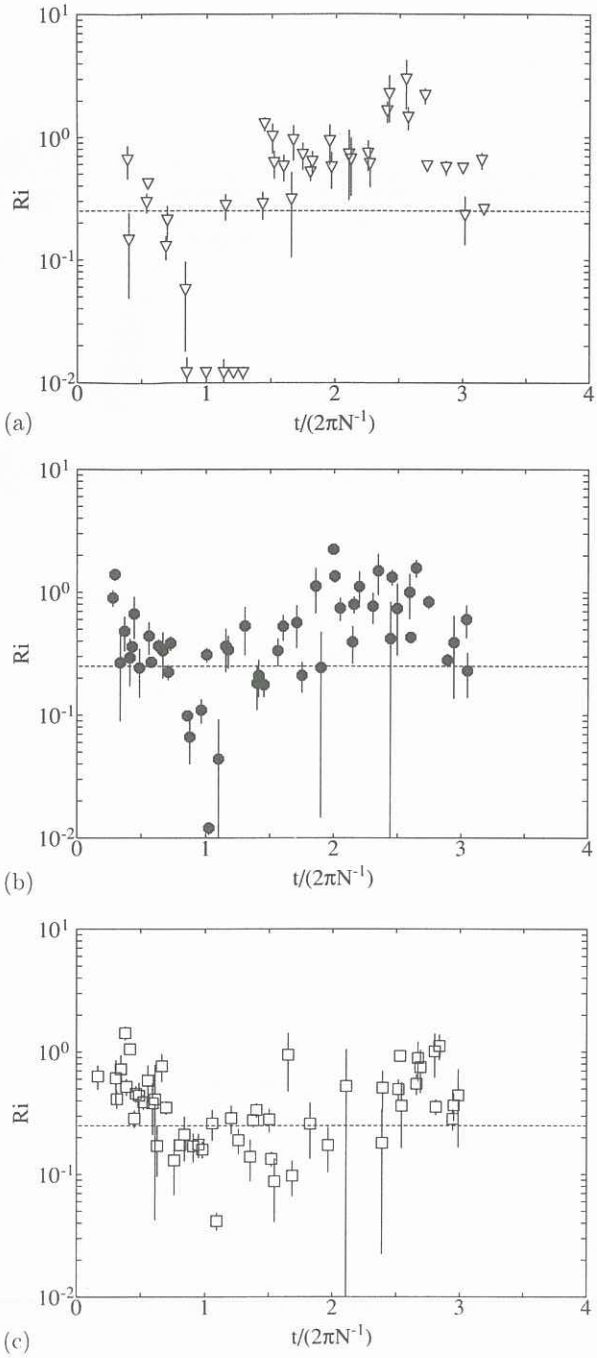

Fig. 5. The average gradient Richardson number for each profile. The time axis is as for Fig. 2. (a) is for paddle amplitude 7°, (b) 10°, and (c) 13°. $Ri < 0$ have been set equal to 0.012. For reference the horizontal dashed line shows $Ri = 0.25$.

flow stagnates prior to decreasing again in the accelerating downslope boundary layer.

The observed ordering of Ri with forcing amplitude in the middle portion of the wave cycle may help to explain the large difference in overall mixing efficiency observed at different forcing amplitudes (Taylor, 1992) compared to the relatively small difference in peak Gr_o (Fig. 2). Thus, shear in the attached up-slope boundary layer flow appears to help maintain turbulence and mixing at the two higher forcing amplitudes.

Discussion

As internal waves broke on a slope the minimum Ri occurred when the stabilising density gradient was minimum and the velocity shear maximum. At this time in the wave cycle there were large scale overturns generated by the wave-induced mean flow. Thus, the evolution of the flow is rather different from that of a conventional shear driven instability. However, the fact that the shear is maximum at the same time suggests that the instability which follows these overturns and drives mixing is not purely convective but is aided by the presence of shear. It was somewhat surprising that there was a much greater contrast in mixing rates at the three forcing amplitudes studied than there was in the magnitudes of the peak values of Gr_o. The present results for Ri suggest that this discrepancy may be explained by additional shear-induced mixing in the attached up slope boundary layer flow which follows the period of largest scale overturning. To test this hypothesis the small scales of the velocity and density fields are being investigated further.

Acknowledgements. J. Imberger and C. Lemckert made useful comments on earlier versions of this paper. The project was supported financially by the Australian Research Council. Centre for Water Research Reference ED–704–JT.

References

Head, M. J. (1983) The use of miniature four-electrode conductivity probes for high resolution measurement of turbulent density or temperature variations in salt-stratified water flows. Ph.D. dissertation, University of California, San Diego, 211pp.

Imberger, J. (1989) Vertical heat flux in the hypolimnion of a lake. *Tenth Australasian Fluid Mechanics Conference*, University of Melbourne, 2.13–2.16.

Imberger, J. and G. N. Ivey (1991) On the nature of turbulence in a stratified fluid. Part 2: application to lakes. *J. Phys. Oceanogr., 21*, 659–680.

Ivey, G. N. and R. I. Nokes (1989) Vertical mixing due to the breaking of critical internal waves on sloping boundaries. *J. Fluid Mech., 204*, 479–500.

Stevens, C. S. and M. J. Coates (1991) A maximised cross-correlation technique for resolving velocity fields in laboratory experiments. Report ED–425–CS, Centre for Water Research, Univ. West. Aust.

Taylor, J. R. (1992) Turbulence and mixing in the boundary layer generated by shoaling internal waves. Submitted to *Dyn. Oceans Atmos.*.

Taylor, J. R. (1992) The energetics of breaking events in a resonantly forced internal wave field. *J. Fluid Mech., 239*. 309 339.

Thorpe, S. A. (1977) Turbulence and mixing in a Scottish loch. *Phil. Trans. R. Soc. London, A 286*, 125–181.

Thorpe, S. A., M. Curé and M. White (1991) The skewness of temperature derivatives in oceanic boundary layers. *J. Phys. Oceanogr., 21*, 428–433.

Turner, J. S. (1979) *Buoyancy effects in fluids*. Cambridge University Press, Cambridge, 368pp.

Willert, C. E. and M. Gharib (1991) Digital particle image velocimetry. *Exp. in Fluids, 10*, 181–193.